Compressible And Incompressible Effects Related With Navier-Stokes Equation

[1]Jai Prakash Singh
[1]Research Scholar
[1]Deptt. Of Mathematics, J.P.University, Chapra

***Abstract* - This paper reveals that the thermal noise implies large fluctuations of the phase-angle difference between the rotors, but synchronization prevails and the ensemble-averaged time dependence of the phase-angle difference agrees well with analytical predictions. Moreover, we demonstrate that compressibility effects lead to longer synchronization times. In addition, the relevance of the inertia terms of the Navier–Stokes equation are discussed, specifically the linear unsteady acceleration term characterized by the oscillatory Reynolds number ReT. We illustrate the continuous breakdown of synchronization with the Reynolds number ReT, in analogy to the continuous breakdown of the scallop theorem with decreasing Reynolds number.**

***keywords* - Navier-Stokes, Reynolds number, compressible, incompressible, etc.**

Introduction

The Multiparticle collision dynamics fluid consists of N point particles of mass m with the positions $\boldsymbol{r}_i$ and velocities $\boldsymbol{v}_i$ ($i = 1, \ldots, N$), which interact with each other by a stochastic, momentum-conserving process. The particle dynamics proceed in two steps—streaming and collision. In the ballistic streaming step, the particle positions are updated *via*

$$\boldsymbol{r}_i(t + h) = \boldsymbol{r}_i(t) + h\boldsymbol{v}_i(t), \tag{1}$$

where h is the collision time step. In the collision step the simulation box is partitioned into cubic cells of length a, in which multiparticle collisions are performed. In the SRD version of MPC,[1] the relative velocity of each particle, with respect to the center-of-mass velocity of the cell, is rotated by a fixed angle α around a randomly oriented axis. Hence, the new velocities are

$$\boldsymbol{v}_i(t + h) = \boldsymbol{v}_{\mathrm{cm}}(t) + \mathbf{R}(\alpha)[\boldsymbol{v}_i(t) - \boldsymbol{v}_{\mathrm{cm}}(t)], \tag{2}$$

where $\mathbf{R}(\alpha)$ is the rotation matrix,[2]

$$\boldsymbol{v}_{\mathrm{cm}} = \frac{1}{N_c}\sum_{i\in\mathrm{cell}} \boldsymbol{v}_i \tag{3}$$

is the center-of-mass velocity, and N_c the total number of particles in the cell. In its original version, MPC violates Galilean invariance. It is restored by a random shift of the collision grid at every step.[3]

The collision rule (2) violates angular momentum conservation, which is associated with a non-symmetric stress tensor. Angular momentum conservation is reestablished on the cell level by a solid-body type rotation of relative velocities after a collision according to

$$\boldsymbol{v}_i(t+h) = \boldsymbol{v}_{\mathrm{cm}}(t) + \mathbf{R}(\alpha)\left[\boldsymbol{v}_i(t) - \boldsymbol{v}_{\mathrm{cm}}(t)\right] - \boldsymbol{r}_{i,c} \times \left[m\mathbf{I}^{-1} \sum_{j\in\mathrm{cell}} \left\{ \boldsymbol{r}_{j,c}(t) \times [\boldsymbol{v}_{j,c}(t) - \mathbf{R}(\alpha)\boldsymbol{v}_{j,c}(t)] \right\} \right], \tag{4}$$

where $\mathbf{I}$ is the moment of inertia tensor of the particles in the center-of-mass reference frame; $\boldsymbol{r}_{i,c}(t)$ and $\boldsymbol{v}_{i,c}(t)$ are the respective relative positions and velocities after streaming, *i.e.*, $\boldsymbol{r}_{i,c} = \boldsymbol{r}_i - \boldsymbol{r}_{\mathrm{cm}}$ and $\boldsymbol{v}_{i,c} = \boldsymbol{v}_i - \boldsymbol{v}_{\mathrm{cm}}$, with the center-of-mass position $\boldsymbol{r}_{\mathrm{cm}}$.

In order to simulate an isothermal fluid, a collision-cell-based, local Maxwellian thermostat is applied, where the relative velocities of the particles in a cell are scaled according to the Maxwell–Boltzmann scaling (MBS) method.

We adopt the rotor model: two beads of radius R_{H} move along circles of radius R, each driven by an active force $\boldsymbol{F}_i$ (*cf.*Fig. 1). The two circles are centered at $\boldsymbol{R}_{i0} = (-1)_i(d/2)\boldsymbol{e}_x$ ($i = 1, 2$), where $\hat{\boldsymbol{e}}_x$ is the unit vector along the x-axis and d the center-to-center distance; both beads are confined in the xy-plane. The trajectories of the bead centers can be expressed as

$$\boldsymbol{R}_i(t) = \boldsymbol{R}_{i0} + (R\cos\varphi_i(t),\ R\sin\varphi_i(t),\ 0)^{\mathrm{T}}, \tag{5}$$

in terms of the phase angles $\varphi_i(t)$. The driving forces

$$\boldsymbol{F}_i(t) = F\hat{\boldsymbol{t}}_i(t) \tag{6}$$

are of equal magnitude and point along the tangents $\hat{\boldsymbol{t}}_i(t)$ of the trajectories, where

$$\hat{\boldsymbol{t}}_i(t) = (-\sin\varphi_i(t), \cos\varphi_i(t), 0)^T. \quad (7)$$

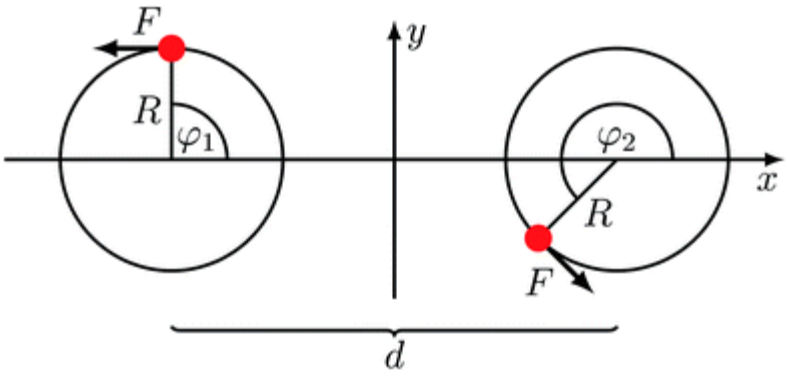

Fig. 1 Model system of hydrodynamically coupled rotors.[4] Two beads move along fixed circular trajectories, each driven by a constant tangential force *F*.

The coupling of the beads with the MPC solvent is established in the collision step.[5] Thereby, the beads are treated as fluid particles with the mass *M*. Thus, in cells with a bead the center-of-mass velocity is given by

$$\boldsymbol{v}_{cm}(t) = \frac{\sum_{i=1}^{N_c} m\boldsymbol{v}_i(t) + M\boldsymbol{V}(t)}{mN_c + M}. \quad (8)$$

The velocity $\boldsymbol{V}(t+h)$ of the bead after a collision follows according to eqn (2) or (4), respectively, taking into account the appropriate mass *M*.

Hence, the phase angles evolve as

$$\varphi_i(t+h) = \varphi_i(t) + \dot{\varphi}_i(t)h + \frac{1}{2}\left(\frac{F}{MR}\right)h^2 \quad (9)$$

between MPC collisions. In a collision, the angular velocities change. The new values after a collision follow from the relation

$$\dot{\varphi}_i(t+h) = \frac{1}{R}\hat{\boldsymbol{t}}_i(t+h)\cdot\boldsymbol{V}_i(t+h). \quad (10)$$

All simulations are performed with the rotation angle $\alpha = 130°$, the mean number of particles per collision cell $\langle N_c \rangle = 10$, and the collision step $h = 10^{-2}\sqrt{ma^2/(k_B\Theta)}$, where Θ is the temperature and k_B the Boltzmann constant. This yields the viscosity $\eta \approx 82.2\sqrt{mk_B\Theta/a^4}$ for the non-angular momentum conserving MPC variant (2).[6] For a rotor, we choose $M = 10m$, which yields the bead diffusion coefficient $D_0/\sqrt{k_B\Theta a^2/m} \approx 0.0023$ and the hydrodynamics radius $R_H = k_B\Theta/(6\pi\eta D_0) \approx 0.28a$ assuming no-slip boundary conditions. The radius of a circle is set to $R = 2a$ and the distance to $d = 5a$ in terms of the MPC length scale. In simulations, forces in the range $F/(k_B\Theta/a) = 10–100$ are considered, which corresponds to the Péclet numbers $\mathrm{Pe} = FR/(k_B\Theta) = 20–200$.

Periodic boundary conditions are applied for the fluid, with a rectangular square–cuboid box of side lengths $L_x = L_y = 100a$ and $L_z = 20a$.

All results presented in the following have been obtained with the non-angular momentum conserving collision rule (2). However, simulations confirm that these results are independent of the applied MPC variant and they agree very well with each other.

Hydrodynamics

As is well established, the hydrodynamic properties of the MPC fluid are excellently described by the linearized Navier–Stokes equations on sufficiently large length and time scales. Moreover, the dynamics of the coupled rotors can be described analytically within the linearized Navier–Stokes equations.[7] In order to establish a link between simulation results and analytical considerations, we will briefly describe the basic hydrodynamic background.

Navier–Stokes equations and MPC fluid

Mass and momentum conservation of an isothermal fluid are expressed by the continuity and the Navier–Stokes equation[8]

$$\frac{\partial\delta\rho}{\partial t} + \nabla\cdot(\rho\boldsymbol{v}) = 0, \quad (11)$$

$$\rho\left(\frac{\partial \boldsymbol{v}}{\partial t}+(\boldsymbol{v}\cdot\nabla)\boldsymbol{v}\right)=\nabla\cdot\boldsymbol{\sigma}+\boldsymbol{f}, \tag{12}$$

respectively. Here, $\rho + \delta\rho(\boldsymbol{r}, t)$ denotes the mass density with its mean value ρ and its (small) fluctuations $\delta\rho(\boldsymbol{r}, t)$ at the position $\boldsymbol{r}$ in space and the time t. $\boldsymbol{v} = \boldsymbol{v}(\boldsymbol{r}, t)$ is the fluid velocity field, $\boldsymbol{f}(\boldsymbol{r}, t)$ a volume force, and $\boldsymbol{\sigma}(\boldsymbol{r}, t)$ the stress tensor. Note that only the mean density ρ will appear throughout the rest of the paper.

For the MPC fluid, the explicit form of the stress tensor depends on the lack or presence of angular momentum conservation during collision. In general, the stress tensor can be expressed as

$$\sigma_{\alpha\beta}=-p\delta_{\alpha\beta}+\sum_{\alpha',\beta'}\eta_{\alpha\beta\alpha'\beta'}\frac{\partial v_{\alpha'}}{\partial r_{\beta'}}, \tag{13}$$

with the pressure p and the Cartesian indices $\alpha, \beta, \alpha', \beta' \in \{x, y, z\}$.

(i) For angular momentum conserving fluids, the standard symmetric stress tensor is obtained

$$\sigma_{\alpha\beta}=-p\delta_{\alpha\beta}+\eta\left(\frac{\partial v_\alpha}{\partial r_\beta}+\frac{\partial v_\beta}{\partial r_\alpha}-\frac{2}{3}\delta_{\alpha\beta}\sum_{\alpha'}\frac{\partial v_{\alpha'}}{\partial r_{\alpha'}}\right), \tag{14}$$

with

$$\eta_{\alpha\beta\alpha'\beta'}=\eta\left(\delta_{\alpha\alpha'}\delta_{\beta\beta'}+\delta_{\alpha\beta'}\delta_{\beta\alpha'}-\frac{2}{3}\delta_{\alpha\beta}\delta_{\alpha'\beta'}\right) \tag{15}$$

in three dimensions. η denotes the shear viscosity. Note, we assume that the bulk viscosity is zero.[9]

(ii) For the non-angular momentum conserving variant of the MPC approach of Sec. 2.1, the non-symmetric tensor is given by

$$\sigma_{\alpha\beta}=-p\delta_{\alpha\beta}+\eta^{\mathrm{k}}\left(\frac{\partial v_\alpha}{\partial r_\beta}+\frac{\partial v_\beta}{\partial r_\alpha}-\frac{2}{3}\delta_{\alpha\beta}\sum_{\alpha'}\frac{\partial v_{\alpha'}}{\partial r_{\alpha'}}\right)+\eta^{\mathrm{c}}\frac{\partial v_\alpha}{\partial r_\beta}, \tag{16}$$

with

$$\eta_{\alpha\beta\alpha'\beta'}=\eta\delta_{\alpha\beta'}\delta_{\beta\alpha'}+\eta^{\mathrm{k}}\left(\delta_{\alpha\alpha'}\delta_{\beta\beta'}-\frac{2}{3}\delta_{\alpha\beta}\delta_{\alpha'\beta'}\right). \tag{17}$$

Here, η_{k} and η_{c} are the kinetic and collisional contribution to the viscosity $\eta = \eta_{\mathrm{k}} + \eta_{\mathrm{c}}$. Alternative expressions for the stress tensor have been used, which differ from eqn (16) by a term with vanishing divergence only and thus yield the same Navier–Stokes equation.

With the stress tensor (16), eqn (12) turns into

$$\rho\left(\frac{\partial \boldsymbol{v}}{\partial t}+(\boldsymbol{v}\cdot\nabla)\boldsymbol{v}\right)=-\nabla p+\eta\Delta\boldsymbol{v}+\frac{\eta^{\mathrm{k}}}{3}\nabla(\nabla\cdot\boldsymbol{v})+\boldsymbol{f}. \tag{18}$$

For angular momentum conserving fluids η_{k} is replaced by η in eqn (18).

Inertia and Reynolds numbers

In order to asses the relevance of the various terms in eqn (18), in particular the time-dependent and non-linear inertia terms, we scale the velocity field by a typical value V, length by L, and time by T, as usual, which yields the equation

$$\mathrm{Re}_{\mathrm{T}}\frac{\partial \boldsymbol{v}'}{\partial t'}+\mathrm{Re}(\boldsymbol{v}'\cdot\nabla')\boldsymbol{v}'=-\nabla' p'+\Delta'\boldsymbol{v}'+\frac{\eta^{\mathrm{k}}}{3\eta}\nabla'(\nabla'\cdot\boldsymbol{v}')+\boldsymbol{f}', \tag{19}$$

where the primed quantities are dimensionless and of ↺ (1). Furthermore, we introduced the Reynolds numbers

$$\mathrm{Re}=\frac{\rho VL}{\eta}=\frac{VL}{\nu}, \tag{20}$$

$$\mathrm{Re}_{\mathrm{T}}=\frac{\rho L^2}{\eta T}=\frac{L^2}{\nu T}, \tag{21}$$

with the kinematic viscosity $\nu = \eta/\rho$. Typically, T is defined as $T = L/V$ which yields $\mathrm{Re}_{\mathrm{T}} = \mathrm{Re}$, and for $\mathrm{Re} \ll 1$ the left hand side of eqn (19) is neglected. In particular, $\mathrm{Re} = 0$ is assumed for microswimmers, which leads to peculiarities in their locomotion as expressed by the well-known scallop theorem.[10]

The oscillatory Reynolds number Re_{T} can be written as $\mathrm{Re}_{\mathrm{T}} = \tau_\nu/T$, with $\tau_\nu = L^2/\nu$. Hence, Re_{T} is the ratio of the viscose time scale τ_ν for shear wave propagation over the distance L and the characteristic system time T. In order to establish proper hydrodynamic interactions, $\tau_\nu/T < 1$ and, hence, $\mathrm{Re}_{\mathrm{T}} < 1$.

Fluctuating hydrodynamics

In the following, we focus on the linearized Navier–Stokes equation and neglect the advection term, *i.e.*, we set Re = 0, but keep the unsteady acceleration term. Moreover, to account for thermal fluctuations inherent in the MPC fluid, we introduce a random stress tensor $\boldsymbol{\sigma}_{\mathrm{R}}(\boldsymbol{r}, t)$. Then, eqn (18) turns into (Landau–Lifshitz Navier–Stokes equation)

$$\rho\frac{\partial \boldsymbol{v}}{\partial t} = -\nabla p + \eta\Delta\boldsymbol{v} + \frac{\eta^{\mathrm{k}}}{3}\nabla\left(\nabla\cdot\boldsymbol{v}\right) + \boldsymbol{f}. \tag{22}$$

The volume force $\boldsymbol{f}$ now consists of a deterministic force $\boldsymbol{f}_{\mathrm{D}}$ and the random force $\boldsymbol{f}_{\mathrm{R}} = \nabla\cdot\boldsymbol{\sigma}_{\mathrm{R}}$. The stress tensor $\boldsymbol{\sigma}_{\mathrm{R}}$ is assumed to be a Gaussian and Markovian stochastic process with the moments

$$\begin{aligned}\left\langle \boldsymbol{\sigma}^{\mathrm{R}}\right\rangle &= 0,\\ \left\langle \sigma^{\mathrm{R}}_{\alpha\beta}\left(\boldsymbol{r},t\right)\sigma^{\mathrm{R}}_{\alpha'\beta'}\left(\boldsymbol{r}',t'\right)\right\rangle &= 2k_{\mathrm{B}}\Theta\eta_{\alpha\beta\alpha'\beta'}\delta\left(\boldsymbol{r}-\boldsymbol{r}'\right)\delta\left(t-t'\right).\end{aligned} \tag{23}$$

$\eta_{\alpha\beta\alpha'\beta'}$ is either given by eqn (15) or (17) depending on the applied MPC procedure.

Taking the divergence of eqn (22) and using the linearized continuity eqn (11) together with the ideal gas equation of state with the velocity of sound $c = \sqrt{k_{\mathrm{B}}\Theta/m}$ for an isothermal system, we obtain the wave equation

$$\left(\Delta - \frac{1}{c^2}\frac{\partial^2}{\partial t^2}\right)p = \nabla\cdot\left(\eta\Delta\boldsymbol{v} + \frac{\eta^{\mathrm{k}}}{3}\nabla\left(\nabla\cdot\boldsymbol{v}\right) + \boldsymbol{f}\right). \tag{24}$$

In Fourier space, eqn (22) and (24) read as

$$\left(-k^2 + \frac{\omega^2}{c^2}\right)\bar{p} = i\boldsymbol{k}\cdot\left(-\eta k^2\bar{\boldsymbol{v}} - \frac{\eta^{\mathrm{k}}}{3}\boldsymbol{k}\boldsymbol{k}^{\mathrm{T}}\bar{\boldsymbol{v}} + \bar{\boldsymbol{f}}\right), \tag{25}$$

$$\rho i\omega\bar{\boldsymbol{v}} = -i\boldsymbol{k}\bar{p} - \eta k^2\bar{\boldsymbol{v}} - \frac{\eta^{\mathrm{k}}}{3}\boldsymbol{k}\boldsymbol{k}^{\mathrm{T}}\bar{\boldsymbol{v}} + \bar{\boldsymbol{f}}, \tag{26}$$

with $k = |\boldsymbol{k}|$ and the argument $(\boldsymbol{k}, \omega)$ of all variables with a bar. In order to solve eqn (25) and (26) we define the longitudinal and transverse projection operators $\boldsymbol{P}_{\mathrm{L}}(\boldsymbol{k}) = \hat{\boldsymbol{k}}\hat{\boldsymbol{k}}$, with the unit vector $\hat{\boldsymbol{k}}$ and the dyadic product $\hat{\boldsymbol{k}}\hat{\boldsymbol{k}}$, and $\boldsymbol{P}_{\mathrm{T}}(\boldsymbol{k}) = 1 - \boldsymbol{P}_{\mathrm{L}}(\boldsymbol{k})$ along with $\bar{\boldsymbol{v}}_{\mathrm{L}} = \boldsymbol{P}_{\mathrm{L}}\bar{\boldsymbol{v}}$ and $\bar{\boldsymbol{v}}_{\mathrm{T}} = \boldsymbol{P}_{\mathrm{T}}\bar{\boldsymbol{v}}$. Using these projection operators, we obtain the solution

$$\bar{\boldsymbol{v}}(\boldsymbol{k},\omega) = \bar{\boldsymbol{v}}_{\mathrm{T}}(\boldsymbol{k},\omega) + \bar{\boldsymbol{v}}_{\mathrm{L}}(\boldsymbol{k},\omega) = \bar{\boldsymbol{Q}}(\boldsymbol{k},\omega)\bar{\boldsymbol{f}} = (\bar{Q}_{\mathrm{T}}(\boldsymbol{k},\omega) + Q_{\mathrm{L}}(\boldsymbol{k},\omega))\bar{\boldsymbol{f}}, \tag{27}$$

where

$$\bar{\boldsymbol{Q}}_{\mathrm{T}}(\boldsymbol{k},\omega) = [i\rho\omega + \eta k_2]^{-1}\boldsymbol{P}_{\mathrm{T}} = \bar{Q}_{\mathrm{T}}(\boldsymbol{k},\omega)\boldsymbol{P}_{\mathrm{T}}, \tag{28}$$

and

$$\begin{aligned}\bar{\boldsymbol{Q}}_{\mathrm{L}}\left(\boldsymbol{k},\omega\right) &= \left[\tilde{\eta}k^2 + \frac{i\rho}{\omega}\left(\omega^2 - k^2c^2\right)\right]^{-1}\boldsymbol{P}_{\mathrm{L}}\\ &= \bar{Q}_{\mathrm{L}}\left(\boldsymbol{k},\omega\right)\boldsymbol{P}_{\mathrm{L}},\end{aligned} \tag{29}$$

with $\tilde{\eta} = \eta + \eta_{\mathrm{k}}/3$. The transverse part of the velocity $\bar{\boldsymbol{v}}_{\mathrm{T}}$ describes shear waves, whereas the longitudinal part $\bar{\boldsymbol{v}}_{\mathrm{L}}$ represents sound waves. Fourier transformation with respect to frequency yields the time-dependent tensors $\boldsymbol{Q}_{\mathrm{T}}(\boldsymbol{k}, t) = Q_{\mathrm{T}}(k, t)\boldsymbol{P}_{\mathrm{T}}$ and $\boldsymbol{Q}_{\mathrm{L}}(\boldsymbol{k}, t) = Q_{\mathrm{L}}(k, t)\boldsymbol{P}_{\mathrm{L},11}$ where

$$Q_{\mathrm{T}}\left(k,t\right) = \frac{1}{2\pi}\int \mathrm{d}\omega\, \mathrm{e}^{i\omega t}\bar{Q}_{\mathrm{T}}\left(\boldsymbol{k},\omega\right) = \frac{1}{\rho}\mathrm{e}^{-\nu k^2 t}. \tag{30}$$

For the longitudinal part, we find

$$Q_{\mathrm{L}}\left(k,t\right) = \frac{1}{\rho}\mathrm{e}^{-k^2\tilde{\nu}t/2}\left[\cos\left(\Omega t\right) - \sqrt{\frac{k^2\tilde{\nu}^2}{4c^2 - k^2\tilde{\nu}^2}}\sin\left(\Omega t\right)\right] \tag{31}$$

for $4c_2 > k_2\tilde{\nu}_2$, and

$$Q_{\mathrm{L}}\left(k,t\right) = \frac{1}{\rho}\mathrm{e}^{-k^2\tilde{\nu}t/2}\left[\cosh\left(\Lambda t\right) - \sqrt{\frac{k^2\tilde{\nu}^2}{k^2\tilde{\nu}^2 - 4c^2}}\sinh\left(\Lambda t\right)\right] \tag{32}$$

for $k^2\tilde{\nu}^2 > 4c^2$. Here, we defined $\tilde{\nu} = \tilde{\eta}/\rho$, $\Omega = k^2\tilde{\nu}\sqrt{4c^2/(k^2\tilde{\nu}^2)-1}/2$, $\Lambda = k^2\tilde{\nu}\sqrt{1-4c^2/(k^2\tilde{\nu}^2)}/2$, and assume $t \geq 0$. We obtain the velocity field $\boldsymbol{v}(\boldsymbol{r}, t)$ by Fourier transformation of eqn (27) and using the convolution theorem

$$\boldsymbol{v}(\boldsymbol{r},t) = \int \mathrm{d}^3 r' \int \mathrm{d}t' \, \boldsymbol{Q}(\boldsymbol{r}-\boldsymbol{r}', t-t') \boldsymbol{f}(\boldsymbol{r}', t'). \tag{33}$$

The Green's function

$$\boldsymbol{Q}(\boldsymbol{r},t) = \int \frac{\mathrm{d}^3 k}{(2\pi)^3} \mathrm{e}^{-i\boldsymbol{k}\cdot\boldsymbol{r}} \boldsymbol{Q}(\boldsymbol{k},t) \tag{34}$$

is known as the dynamical Oseen tensor. In general, the matrix elements of $\boldsymbol{Q}(\boldsymbol{r}, t)$ can be expressed as ($r = |\boldsymbol{r}|$)

$$Q_{\alpha\beta}(\boldsymbol{r},t) = \frac{1}{\rho}\left(A(r,t)\delta_{\alpha\beta} - B(r,t)\frac{r_\alpha r_\beta}{r^2} \right) \tag{35}$$

in real space, for both, the transversal and longitudinal part, *i.e.*, $A = A_T + A_L$ and $B = B_T + B_L$. For the transverse part, the closed expressions

$$\begin{aligned} A_T(r,t) &= \left(1+\frac{2\nu t}{r^2}\right) f(r,t) - \frac{g(r,t)}{r^2}, \\ B_T(r,t) &= \left(1+\frac{6\nu t}{r^2}\right) f(r,t) - \frac{3g(r,t)}{r^2}, \\ f(r,t) &= \frac{1}{(4\pi\nu t)^{3/2}} \exp\left(-\frac{r^2}{4\nu t}\right), \\ g(r,t) &= \frac{1}{4\pi r} \mathrm{erf}\left(\frac{r}{\sqrt{4\nu t}}\right) \end{aligned} \tag{36}$$

have been derived.[12] For the longitudinal part, we obtain the integral representation $A_L = I_2$ and $B_L = 3I_2 - 2I_1$, with

$$\begin{aligned} I_1 &= \frac{\rho}{4\pi^2 r} \int_0^\infty \mathrm{d}k \, k Q_L(k,t) \sin(kr), \\ I_2 &= \frac{\rho}{2\pi^2 r^2} \int_0^\infty \mathrm{d}k \, Q_L(k,t) \left[\frac{\sin(kr)}{kr} - \cos(kr) \right]. \end{aligned} \tag{37}$$

Conclusions

We find that the presence of the linear unsteady acceleration term in the Navier–Stokes equation leads to synchronization of the rotational motion. Synchronization even prevails in the presence of thermal fluctuations, as shown by our mesoscale simulations exploiting the MPC method. Thereby, the simulation results are well described by our mean-field analytical theory. Fluid compressibility affects the synchronization time over a certain range of Péclet numbers. Thereby, compressibility implies larger synchronization times compared to incompressible fluids. This is related to the instantaneous propagation of hydrodynamics in incompressible fluids.

References

1. R. Stocker and W. M. Durham, *Science*, 2009, **325**, 400–402.
2. M. Polin, I. Tuval, K. Drescher, J. P. Gollub and R. E. Goldstein, *Science*, 2009, **325**, 487–490 .
3. E. Lauga and T. R. Powers, *Rep. Prog. Phys.*, 2009, **72**, 096601.
4. B. Afzelius, *Science*, 1976, **193**, 317–319.
5. Q. Wang, J. Pan and W. J. Snell, *Cell*, 2006, **125**, 549 .
6. J. H. E. Cartwright, O. Piro and I. Tuval, *Proc. Natl. Acad. Sci. U. S. A.*, 2004, **101**, 7234–7239.
7. B. Qian, H. Jiang, D. A. Gagnon, K. S. Breuer and T. R. Powers, *Phys. Rev. E: Stat., Nonlinear, Soft Matter Phys.*, 2009, **80**, 061919 .
8. R. E. Goldstein, M. Polin and I. Tuval, *Phys. Rev. Lett.*, 2009, **103**, 168103 .
9. K. Drescher, R. E. Goldstein, N. Michel, M. Polin and I. Tuval, *Phys. Rev. Lett.*, 2010, **105**, 168101.
10. J. S. Guasto, K. A. Johnson and J. P. Gollub, *Phys. Rev. Lett.*, 2010, **105**, 168102 .
11. R. E. Goldstein, M. Polin and I. Tuval, *Phys. Rev. Lett.*, 2011, **107**, 148103
12. E. Lauga and R. E. Goldstein, *Phys. Today*, 2012, **65**, 30